Biogeosciences, 11, 6553–6571, 2014
www.biogeosciences.net/11/6553/2014/
doi:10.5194/bg-11-6553-2014

Biogeosciences Open Access

Terrestrial cycling of $^{13}CO_2$ by photosynthesis, respiration, and biomass burning in SiBCASA

I. R. van der Velde[1], J. B. Miller[2,3], K. Schaefer[4], G. R. van der Werf[5], M. C. Krol[1], and W. Peters[1,6]

[1]Meteorology and Air Quality, Wageningen University, Wageningen, the Netherlands
[2]NOAA Earth System Research Laboratory, Boulder, Colorado, USA
[3]CIRES, University of Colorado, Boulder, Colorado, USA
[4]National Snow and Ice Data Center, University of Colorado, Boulder, Colorado, USA
[5]Faculty of Earth and Life Sciences, VU University, Amsterdam, the Netherlands
[6]Centre for Isotope Research, University of Groningen, Groningen, the Netherlands

Correspondence to: I. R. van der Velde (ivar.vandervelde@wur.nl)

Received: 22 November 2013 – Published in Biogeosciences Discuss.: 3 January 2014
Revised: 8 May 2014 – Accepted: 18 June 2014 – Published: 1 December 2014

Abstract. We present an enhanced version of the SiBCASA terrestrial biosphere model that is extended with (a) biomass burning emissions from the SiBCASA carbon pools using remotely sensed burned area from the Global Fire Emissions Database (GFED), (b) an isotopic discrimination scheme that calculates ^{13}C signatures of photosynthesis and autotrophic respiration, and (c) a separate set of ^{13}C pools to carry isotope ratios into heterotrophic respiration. We quantify in this study the terrestrial exchange of CO_2 and $^{13}CO_2$ as a function of environmental changes in humidity and biomass burning.

The implementation of biomass burning yields similar fluxes as CASA-GFED both in magnitude and spatial patterns. The implementation of isotope exchange gives a global mean discrimination value of 15.2 ‰, ranges between 4 and 20 ‰ depending on the photosynthetic pathway in the plant, and compares favorably (annually and seasonally) with other published values. Similarly, the isotopic disequilibrium is similar to other studies that include a small effect of biomass burning as it shortens the turnover of carbon. In comparison to measurements, a newly modified starch/sugar storage pool propagates the isotopic discrimination anomalies to respiration much better. In addition, the amplitude of the drought response by SiBCASA is lower than suggested by the measured isotope ratios. We show that a slight increase in the stomatal closure for large vapor pressure deficit would amplify the respired isotope ratio variability. Our study highlights the importance of isotope ratio observations of ^{13}C to assess and improve biochemical models like SiBCASA, especially with regard to the allocation and turnover of carbon and the responses to drought.

1 Introduction

A key challenge in current carbon cycle research is to estimate the terrestrial and ocean carbon fluxes and to understand their variability. The accumulation of atmospheric CO_2 represents the sum of all sources and sinks and is currently widely used to close the carbon budget. For example, in the year 2010, 9.1 ± 0.5 Pg C (i.e., 10^{15} g) was emitted to the atmosphere as a result of fossil fuel emissions. Land use change added another 0.9 ± 0.7 Pg C to the atmosphere. The sum of these emissions together put an additional burden of CO_2 in the atmosphere (5.0 ± 0.2 Pg C), with the remainder taken up by the terrestrial biosphere and oceans (Peters et al., 2012). How the sink can be partitioned among ocean and land remains hard to quantify.

Fortunately, as more and more isotope ratio observations become available, we now have the opportunity to use ^{13}C to tell us more about the different exchange processes of carbon absorbed by terrestrial biosphere and oceans. For example, measurements of the $^{13}C/^{12}C$ ratio in atmospheric CO_2 (designated as δ_a) have been used as an additional tracer alongside mole fractions of CO_2 (e.g., Keeling and Revelle, 1985; Siegenthaler and Oeschger, 1987; Keeling et al., 1989;

Nakazawa et al., 1993; Tans et al., 1993; Ciais et al., 1995; Rayner et al., 2008; Alden et al., 2010). Plants assimilate the heavier $^{13}CO_2$ molecules less efficiently than $^{12}CO_2$ (by about 2 %), whereas net ocean exchange does not significantly discriminate against the heavier isotope (just 0.2 %). The most dominant photosynthetic pathways in the terrestrial biosphere (C_3) also discriminates significantly more than the less common (C_4) pathway. Therefore, patterns in atmospheric CO_2 and δ_a together can potentially provide more insights on the carbon fluxes.

The heterogeneous structure of the terrestrial biosphere and its response to weather and climate make CO_2 and $^{13}CO_2$ exchange variable in space and time. The extent to which plants discriminate against $^{13}CO_2$ is strongly dependent on environmental conditions that act on the photosynthesis. Atmospheric humidity, precipitation, and soil moisture are factors that, determine the stomatally induced variations in isotopic discrimination (Farquhar et al., 1989; Wingate et al., 2010). In addition, the global distribution of C_3 and C_4 plants affects the global mean discrimination strongly (Still et al., 2003). Carbon that respires back to the atmosphere is heavier in ^{13}C than newly assimilated carbon and acts as an additional flux of $^{13}CO_2$ molecules towards the atmosphere (disequilibrium flux). This stems from a constant dilution of δ_a by isotopically depleted CO_2 from fossil fuel combustion (also known as the Suess effect; Suess, 1955; Keeling, 1979). Errors in the representation of disequilibrium fluxes can lead to errors in the estimated land–ocean mean flux partitioning, as well as in the estimated variability of each sink. For example, an underestimation in the calculated isotopic signature of the carbon pools or their turnover could cause an underestimate of the disequilibrium flux, requiring a change in the estimated partitioning of the net biosphere flux and ocean flux. Much effort therefore goes into improving the realism of ocean and biosphere carbon exchange and its impact on the isotopic ratio.

A similar argument can be made for flux variability. Alden et al. (2010) and van der Velde et al. (2013) showed that observed variability in $^{13}CO_2$ is difficult to reproduce when ocean variability is assumed low. To close the atmospheric ^{13}C budget, the variability in the biosphere must be larger than currently accounted for in SiBCASA (van der Velde et al., 2013). Therefore, the current lack of understanding of the atmospheric budget is an important justification to explore isotope exchange with the atmosphere and the terrestrial biosphere in more detail.

In the past, significant attention has been paid to realistically simulate the seasonal and spatial variations of C_3 and C_4 plant discrimination, and the coupling between carbon assimilation and leaf CO_2 concentration on monthly time intervals (e.g., Lloyd and Farquhar, 1994; Fung et al., 1997). In recent studies, more detailed process descriptions have been used to estimate plant discrimination (e.g., Kaplan et al., 2002; Suits et al., 2005), but these models could not simulate the isotopic disequilibrium because they lacked descriptions of terrestrial carbon pools. Scholze et al. (2003 and 2008) developed a full terrestrial cycling framework of CO_2 and $^{13}CO_2$ in the Lund–Potsdam–Jena dynamic vegetational model (LPJ). This model included the isotopic fractionation model of Kaplan et al. (2002) and above- and belowground biogeochemical pools to store the total carbon and ^{13}C in consistent ratios.

Presented here are several novel additions to the SiBCASA biosphere/biogeochemical model: firstly, a representation of biomass burning emissions that is consistent with the predicted amount of standing biomass, secondly, a framework of ^{13}C exchange, and finally, a modified storage pool to simulate more accurately isotopic signals in respired CO_2. We investigate how the new model performs compared to similar models and observations, and where there is need for improvements. Our efforts build upon the work of Schaefer et al. (2008), who developed the original SiBCASA terrestrial biosphere model that combines the prediction of photosynthesis with the allocation of biomass. We included an isotopic discrimination parameterization scheme from Suits et al. (2005) to simulate isotopic composition at a high spatial and temporal resolution. Our aim is threefold: (1) to evaluate SiBCASA isotopic discrimination with published literature; (2) to evaluate SiBCASA return fluxes to the atmosphere, the isotopic disequilibrium and biomass burning; and (3) to simulate the short-term plant discrimination and respiration response to environmental conditions, and compare those with observations.

2 Methodology

2.1 SiBCASA model

The SiBCASA model (Schaefer et al., 2008) combines two biogeochemical process models in a single framework. The biophysical part of the model is based on the Simple Biosphere model, version 3 (SiB; Sellers et al., 1996a), with the carbon biogeochemistry from the Carnegie–Ames–Stanford approach (CASA; Potter et al., 1993) model. The joint model framework calculates at 10 min time steps and at a spatial resolution of $1^\circ \times 1^\circ$ the exchange of carbon, energy, and water. In the canopy air space, the CO_2 concentration, temperature, and humidity are calculated as prognostic variables (Vidale and Stockli, 2005). Effects of rainfall, snow cover, and aerodynamic turbulence are included in the computation of the latent and sensible heat fluxes (Sellers et al., 1996a).

For plant photosynthesis, SiBCASA uses the Ball–Berry stomatal conductance model as modified by Collatz et al. (1991) coupled to a modified version of the Farquhar et al. (1980) C_3 enzyme kinetic model and the Collatz et al. (1992) C_4 photosynthesis model. Leaf photosynthesis is scaled to the canopy level using the absorbed fraction of photosynthetically active radiation (fPAR) derived from remotely sensed AVHRR (Advanced Very High Resolution

Radiometer) normalized difference vegetation index (NDVI; Sellers et al., 1994, 1996a, b).

The photosynthetic carbon flux is calculated for two physiological plant types (currently C_3 and C_4). The global $1° \times 1°$ map with the fraction of C_4 plants is provided by Still et al. (2003), a static map that represents the mean C_4 distribution for 1980s and 1990s. For the grid cells that contain a fraction of both C_3 and C_4 plant types, the uptake is computed separately from each of the plant types, which is subsequently combined into the carbon pools depending on their fractional coverage to get grid-cell-average fluxes. Respiration flux is calculated from these combined pools.

As displayed in Fig. 1a, the total carbon ($^{13}C + ^{12}C$) that is photosynthesized is allocated to a series of different live carbon pools (leaf, root, wood), surface litter pools (coarse woody debris, metabolic, structural, and microbial) and layered soil pools (metabolic, structural, microbial, slow, and armored). The amount of carbon in each of the 14 biogeochemical pools is solved prognostically as a first-order linear differential equation depending on gains from other pools, losses to other pools, and respiration losses due to (heterotrophic) microbial decay and (autotrophic) plant growth (Schaefer et al., 2008). The leaf pool is somewhat special because its carbon stocks are computed semi-prognostically. This means that the photosynthesis calculations are constrained by remotely sensed leaf area and the leaf pool is prognostic but can only vary within limits of remotely sensed leaf area.

$^{13}CO_2$ fluxes are computed in the isotopic discrimination model that we implemented in SiBCASA (see Sect. 2.2). We keep the ^{13}C stocks separated from the total carbon stocks by defining 14 additional biogeochemical pools for ^{13}C alone. Similar to total carbon, ^{13}C is transferred from one pool to another as shown in Fig. 1a. No discrimination effects are considered for transfers of carbon between pools and during respiration. The average turnover times, as well as the scaling factors for temperature, freezing, and moisture, were taken from the original SiBCASA scheme. The separation of C_3 and C_4 pools has not yet been realized. That means that carbon resulting from C_3 and C_4 photosynthesis is combined in a fractional weighted average to the same set of C pools. This is not ideal, because we would ignore the fact that C_3 and C_4 plants have their own turnover and environmental responses. We performed test simulations where we prescribed 100 % coverage of either C_3 or C_4 photosynthesis depending on the fractional dominance in each grid, and this showed only a small reduction (~ 4 %) in the global isotopic disequilibrium flux.

To improve simulated ^{13}C dynamics, we added a second storage pool to separately simulate sugar and starch allocation. This type of configuration is required to improve the exchange of ^{13}C signatures and will be discussed in detail in Sect. 3.3. Originally, SiBCASA was designed with a single storage pool to represent the total amount of nonstructural carbohydrates (sugars and starch). Of this storage, only the sugar portion, mainly in the form of sucrose, is readily available for plant growth (Schaefer et al., 2008). Sugars can be converted into starch and back if needed, but the fraction of sugars in the storage pool is typically 5 to 30 % depending on the plant species and time of year (Piispanen et al., 2001; Barbaroux et al., 2002; Gaucher et al., 2005). Based on observations of oak trees, the model assumed a sugar fraction of 10 % for all biomes (Schaefer et al., 2008). Because only 10 % of the storage pool is available for growth, the effective

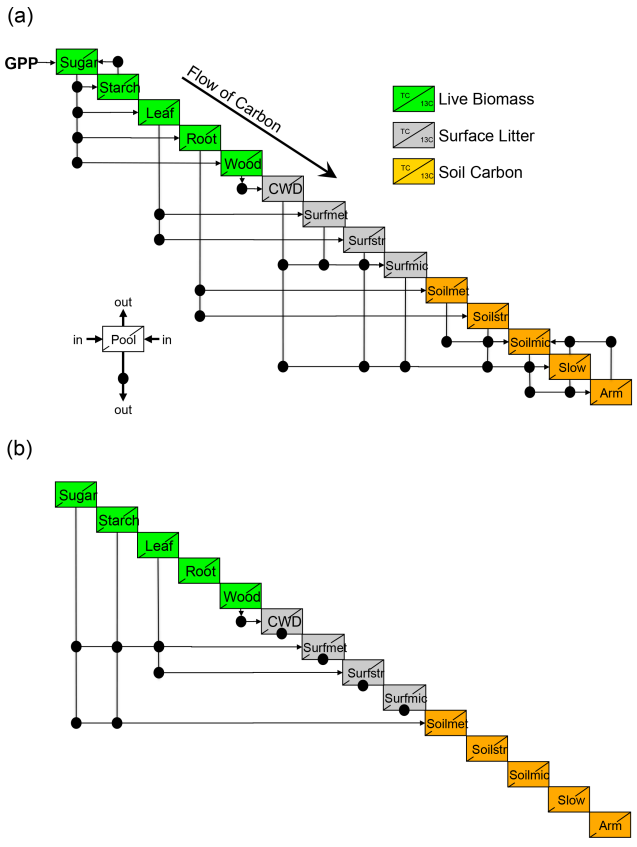

Figure 1. The modified SiBCASA pool configuration **(a)**, where each box represents a total carbon (TC) and ^{13}C pool. Carbon generally flows from upper left to lower right: vertical lines are losses from each pool; horizontal arrows are gains to each pool; and dots represent the transfer of carbon from one pool to another, where a fraction is lost to the atmosphere as respiration. GPP minus the canopy respiration puts sugars into the sugar pool, which becomes available for growth and maintenance of leafs, roots, and wood. Part of the sugar and starch is transferred from one another to keep the ratio between sugar and starch around 1 : 9. Dying of biomass is mimicked by transferring carbon to the structural, metabolic, and microbial surface and soil pools. The autotrophic respiration results from growth and maintenance in the live biomass pools and heterotrophic respiration results from microbial decay in the surface litter and soil carbon pools. The other pool configuration displays the flow of carbon introduced by fire disturbances **(b)**. Vertical lines represent pool losses, horizontal lines represent pool gains, and dots represent the TC and ^{13}C fire losses to the atmosphere.

pool turnover is actually 10 times greater (~ 70 days) than the reference turnover of 7 days as dictated by decay rate formulation (Eq. 9) in Schaefer et al. (2008). This not an error but a consequence of having a combined storage pool of sugars and starch, of which only a fraction is available for plant growth. With the new storage pool we separated the sugar from starch by defining two storage pools. Using prescribed turnover rates for the transfer of sugar to starch (7 days) and the transfer of starch to sugar (63 days), we allow carbon to transform back and forth from one pool to the other to keep the ratio between sugar and starch close to 1 : 9. Carbon used for plant growth comes from the sugar storage pool, which keeps the effective turnover time close to 7 days, but we still retain a similar amount of carbon allocation and carbon exchange. The new double storage pool configuration is displayed in Fig. 1a and b. This configuration is especially required to improve the simulation of coupled ^{12}C and ^{13}C dynamics, but is not necessarily needed when simulating the exchange of total carbon alone.

2.2 Isotopic discrimination

Inherited from the SiB2.5 model is the CFRAX (carbon fractionation) scheme to calculate the $^{13}C/^{12}C$ isotopic ratios in the terrestrial exchange fluxes of CO_2 (Suits et al., 2005). These ratios are the result of several discrimination effects during the photosynthetic uptake of CO_2, when plants favor taking up the more abundant $^{12}CO_2$ molecules rather than the heavier $^{13}CO_2$ molecules. From atmosphere to plant interior, SiBCASA identifies three transport stages, where at each stage the CO_2 concentration is slightly altered due to a resistance. Similarly, these stages are also associated with discrimination against $^{13}CO_2$. These discrimination effects are expressed as Δ in per mill, which is indicative of how much the isotopic ratio will change from one location to the next. See the Appendix for a more detailed explanation on how to interpret the notation of isotopes and discrimination in this publication.

The total discrimination for C_3 plants (Δ_{C_3}) is given by a weighted sum of all the transfer stages that are associated with photosynthesis (Farquhar, 1983):

$$\Delta_{C_3} = \Delta_b \left(\frac{C_a - C_s}{C_a}\right) + \Delta_s \left(\frac{C_s - C_i}{C_a}\right) + \left(\Delta_{diss} + \Delta_{aq}\right)\left(\frac{C_i - C_c}{C_a}\right) + \Delta_f \left(\frac{C_c}{C_a}\right), \quad (1)$$

where the subscripts a, s, i, and c of C represent the CO_2 concentrations in canopy air space, leaf boundary layer, stomatal cavity, and the chloroplasts, respectively. The separate isotope effects are constant and determined from theoretical calculations and laboratory experiments (Craig, 1953; Farquhar, 1983; Mook et al., 1974; O'Leary, 1984). Two of them are related to molecular diffusion from canopy air space to leaf boundary layer ($\Delta_b = 2.9$ ‰) and molecular diffusion through the leaf stomata ($\Delta_s = 4.4$ ‰). Subsequently, smaller isotope effects occur during the dissolution of CO_2 in mesophyll and transport to the chloroplast ($\Delta_{diss} = 1.1$ and $\Delta_{aq} = 0.7$ ‰). The largest isotope effect is associated with the fixation of CO_2 by the enzyme rubisco and a small fraction by the phosphoenol pyruvate carboxylase (PEPC) enzyme in the chloroplast ($\Delta_f = 28.2$ ‰). A schematic representation of Eq. 1 in relation to the flow of carbon is given in Fig. 3 in Suits et al. (2005).

Because the separate isotope effects are assumed constant, variability in Δ_{C3} depends on the concentration gradient between the canopy air space and the leaf interior, which depends on the opening and closing of leaf stomata (stomatal conductance). For instance, water deficiency would generally close the leaf stomata and decrease the stomatal conductance, which results in a drop of the plant interior CO_2 concentrations (C_i and C_c). Consequently, a large CO_2 gradient will exist between the ambient atmosphere and interior plant. The discrimination term associated with CO_2 fixation by rubisco (last term in Eq. 1) will disappear as the ratio C_c/C_a approaches zero. However, at the same time, more weight will be assigned to discrimination associated with molecular diffusion through the leaf stomata. When there is no water stress, the opposite will happen. Stomata remain open, and therefore a small CO_2 gradient will exist, which keeps the C_c/C_a ratio large, and thus more weight is assigned to the rubisco fixation stage.

For C_4 plants, we assume that all of the available carbon is fixed by PEPC. Therefore, similar to Suits et al. (2005), we only assume an isotopic effect associated with molecular diffusion at the leaf stomata, i.e., $\Delta_{C4} = 4.4$ ‰. Brüggemann et al. (2011) discuss several other possible fractionation steps associated with the transport of organic matter between different plant tissues; however such processes are not included in our model since the availability of such data remains scarce. Despite lab and field evidence for fractionation effects during allocation and respiration (Bowling et al., 2008), these effects have not yet been included in SiBCASA. The isotopic discrimination value (denoted as Δ, which can refer to either C_3 or C_4), is used to compute the ^{13}C and ^{12}C flux ratios of total carbon assimilation (F_a), canopy respiration ($F_{respcan}$), and net assimilation ($F_n = F_a - F_{respcan}$). The fluxes are given in $\mu mol\, m^{-2}\, s^{-1}$.

The $^{13}C/^{12}C$ ratio in the current net assimilated plant material (R_n) is determined by the relationship between discrimination Δ and the isotopic ratio of the atmosphere (R_{atm}),

$$R_n = \frac{R_{atm}}{\left(\frac{\Delta}{1000} + 1\right)}, \quad (2)$$

and is discussed in more detail in the Appendix. Subsequently, the ^{13}C and ^{12}C net assimilation rates are calculated by

$$^{13}F_n = \frac{R_n \cdot F_n}{1 + R_n}, \quad (3)$$

$$^{12}F_{\mathrm{n}} = \frac{F_{\mathrm{n}}}{1+R_{\mathrm{n}}}. \quad (4)$$

The latter two fluxes are calculated separately for physiological plant types C_3 and C_4 and, in combination with the prescribed fraction of C_3 plants (β), a grid-cell-averaged flux is calculated:

$$^{13}F_{\mathrm{n}} = {}^{13}F_{\mathrm{n,c3}} \cdot \beta + {}^{13}F_{\mathrm{n,c4}} \cdot (1-\beta), \quad (5)$$

$$^{12}F_{\mathrm{n}} = {}^{12}F_{\mathrm{n,c3}} \cdot \beta + {}^{12}F_{\mathrm{n,c4}} \cdot (1-\beta). \quad (6)$$

To diagnose monthly or daily averages of the total discrimination, Δ must be an assimilation-weighted average since discrimination at night, when photosynthesis is zero, makes no sense. Therefore, over t time steps, we compute for each land point:

$$\Delta_{\mathrm{month}} = \frac{\sum^{\mathrm{t}} \Delta_{\mathrm{t}} \cdot F_{\mathrm{a},t}}{\sum^{\mathrm{t}} F_{\mathrm{a},t}}. \quad (7)$$

2.3 Disequilibrium flux

A so-called disequilibrium flux exists because of a long-term drawdown of the atmospheric $^{13}C/^{12}C$ ratio due to fossil fuel emissions of isotopically light CO_2 (e.g., Francey et al., 1999). Therefore, the older carbon that is released to the atmosphere is richer in ^{13}C compared to the carbon that is currently taken up by the oceans and land. For the terrestrial biosphere, this isotopic difference is designated as the isodisequilibrium forcing coefficient (Alden et al., 2010), and can be separately defined for biological respiration, $I_{\mathrm{ba}} = \delta_{\mathrm{ba}} - \delta_{\mathrm{ab}}$, and for biomass burning, $I_{\mathrm{fire}} = \delta_{\mathrm{fire}} - \delta_{\mathrm{ab}}$ (van der Velde et al., 2013). These isotopic differences are scaled by large gross fluxes: F_{ba} for biological respiration and F_{fire} for biomass burning.

The total isotopic disequilibrium flux from the terrestrial biosphere D_{bio} is defined as

$$\begin{aligned} D_{\mathrm{bio}} &= F_{\mathrm{ba}}[\delta_{\mathrm{ba}} - \delta_{\mathrm{ab}}] + F_{\mathrm{fire}}[\delta_{\mathrm{fire}} - \delta_{\mathrm{ab}}] \quad (8)\\ &= F_{\mathrm{ba}} I_{\mathrm{ba}} + F_{\mathrm{fire}} I_{\mathrm{fire}}, \end{aligned}$$

where the fluxes F_{ba} and F_{fire} are given in $\mu\mathrm{mol\,m^{-2}\,s^{-1}}$ for each grid cell. The monthly isotopic signatures associated with respiration (δ_{ba}), biomass burning (δ_{fire}) and uptake (δ_{ab}) are determined with the use of Eq. (A2), i.e.,

$$\delta_{\mathrm{ba}} = 1000 \times \left(\frac{^{13}F_{\mathrm{ba}}/^{12}F_{\mathrm{ba}}}{R_{\mathrm{std}}} - 1 \right), \quad (9)$$

$$\delta_{\mathrm{fire}} = 1000 \times \left(\frac{^{13}F_{\mathrm{fire}}/^{12}F_{\mathrm{fire}}}{R_{\mathrm{std}}} - 1 \right), \quad (10)$$

$$\delta_{\mathrm{ab}} = 1000 \times \left(\frac{^{13}F_{\mathrm{a}}/^{12}F_{\mathrm{a}}}{R_{\mathrm{std}}} - 1 \right). \quad (11)$$

2.4 Biomass fire scheme

We introduce fire combustion of total carbon and ^{13}C in SiBCASA, which is largely based on the work of van der Werf et al. (2003 and 2010). Our calculated fire emissions are driven by multiple remotely sensed burned-area products combined in the Global Fire Emissions Database (GFED) (Giglio et al., 2010). The burned area is given in hectares per month and spans the time period from July 1996 through to the end of 2011. Most of the burned area is estimated using Moderate Resolution Imaging Spectroradiometer (MODIS) surface reflectance imagery. The data set is extended prior to MODIS with fire observations from the Tropical Rainfall Measuring Mission (TRMM) Visible and Infrared Scanner (VIRS) and Along-Track Scanning Radiometer (ATSR). To make GFED burned area serve as input for our model, its original $0.5^\circ \times 0.5^\circ$ grid is aggregated to a total of 14 538 $1^\circ \times 1^\circ$ SiBCASA land points. Furthermore, the burned area is transformed to a scaling factor, A, by dividing the burned area (BA) by the area (GA) of each grid cell and the number of seconds per month (S):

$$A = \frac{\mathrm{BA}}{\mathrm{GA} \cdot S}. \quad (12)$$

The burning rate (A, $\mathrm{s^{-1}}$) together with the tree mortality rates (M, rate that relates to the density of trees in a biome), carbon stocks (C) and pool-dependent combustion completeness factors (E, the fraction of biomass available for combustion for each pool E_p) determine the combustion flux of total carbon and ^{13}C:

$$F_{\mathrm{fire}} = A \cdot M \sum^{p} C_p \cdot E_p, \quad (13)$$

$$^{13}F_{\mathrm{fire}} = A \cdot M \sum^{p} {}^{13}C_p \cdot E_p, \quad (14)$$

where F_{fire} and $^{13}F_{\mathrm{fire}}$ represent the fire flux per grid cell per time step (given in $\mu\mathrm{mole\,m^{-2}\,s^{-1}}$) summed over the p number of aboveground and fine-litter pools. The numbers used for the combustion completeness and tree mortality are given in Table 1. The carbon flow chart for fires is given in Fig. 1b. We assume that only aboveground biomass and fine litter on the surface are directly affected by fires. Part of the carbon that is not combusted is regarded as dead biomass and is subsequently transferred from the aboveground pools to the fine-litter pools. The uncombusted carbon in the fine-litter pools is not further transferred. Peat burning (Page et al., 2002) and organic soil carbon combustion in the boreal region are neglected and we made no distinction between ground fires and crown fires. In this study we used the burned-area product from GFEDv3, but confirmed that the differences to the newer GFEDv4 burned area are small.

2.5 Experimental setup

SiBCASA was run globally from 1851 through 2009. At the start of the simulation we assumed an approximate steady

Table 1. Combustion completeness fractions for different biomes and carbon pools. The tree mortality fraction is given in the last column. Both quantities are chosen accordingly to represent the biome mean value. CWD stands for coarse woody debris, and surfmet, surfstr, and surfmic stand for surface metabolic, surface structural, and surface microbial, respectively.

Biomes	Storage	Leaf	Wood	CWD	Surfmet	Surfstr	Surfmic	Mortality
tropical forests	0.9	0.9	0.5	0.2	0.9	0.9	0.9	0.9
deciduous forests	0.8	0.8	0.2	0.4	0.8	0.8	0.8	0.6
mixed deciduous forests	0.8	0.8	0.2	0.4	0.8	0.8	0.8	0.6
taiga forest, boreal forest	0.8	0.8	0.2	0.4	0.8	0.8	0.8	0.6
mixed taiga forest, boreal forest	0.8	0.8	0.2	0.4	0.8	0.8	0.8	0.6
mixed trees and grasslands	0.9	0.9	0.3	0.5	0.9	0.9	0.9	0.05
pure grasslands	0.9	0.9	0.3	0.9	0.9	0.9	0.9	0.01
dry grasslands	0.9	0.9	0.3	0.9	0.9	0.9	0.9	0.01
tundra	0.8	0.8	0.2	0.4	0.8	0.8	0.8	0.6
desert	0.9	0.9	0.3	0.9	0.9	0.9	0.9	0.01
agriculture	0.9	0.9	0.3	0.9	0.9	0.9	0.9	0.01

state in the carbon and ^{13}C pools (NEE ≈ 0), which is an assumption that is often made for biogeochemical models since observations of biomass are not available from that era (Schaefer et al., 2008). Actual driver data (meteorology, NDVI, burned area) were used only for the 1997–2009 period. Before 1997, we drive SiBCASA with randomly ordered input fields taken from our available 13 yr input database to ensure that meteorology, NDVI, and burned area come from the same year and month and are thus internally consistent. That means that any variability from long-term climate change effects, such as rise in global temperature, are not included in these model spin-up periods. The monthly δ_a observational record spans the 1850–2009 period simulated and each year in SiBCASA thus has realistic atmospheric δ_a values, which allows for us to simulate the disequilibrium between biosphere and atmosphere over time (note that climate-imposed changes are not accounted for). The monthly record is based on ice-core measurements (Francey et al., 1999) and from 1989 onward based on atmospheric observations. For the past changes in atmospheric CO_2 concentration, we use a curve fit to observed global CO_2 concentrations from the ice core from Taylor Dome (Indermuhle et al., 1999) and the Globalview data product (Masarie and Tans, 1995).

Two different global simulations are performed: (1) the ISOVAR simulation (we use the same designation as Scholze et al. (2003, 2008) and van der Velde et al. (2013)) includes the dynamic discrimination scheme and (2) the ISOVAR simulation without fire fluxes (ISOVAR-NF, *No Fires*). Between ISOVAR and ISOVAR-NF, the total CO_2 exchange remains almost the same because the excluded fire disturbances in ISOVAR-NF are compensated for by increased respiration. All simulations include the same prescribed records of atmospheric CO_2 and δ_a, the same C_3/C_4 distribution, and the same SiBCASA climate driver files as described above.

3 Results

3.1 ^{13}C signatures in atmosphere–biosphere exchange

The largest spatial differences in the global annual plant discrimination (assimilation-weighted) are determined by the C_3/C_4 plant distribution (Fig. 2a). Regions with lower values of discrimination correspond to the dominant presence of C_4 plants, such as the South American grasslands, African subtropical savannas, northern Australia, and North American crop fields. Smaller differences in discrimination, within C_3 dominant areas, are caused by climate conditions, water availability and relative humidity. These parameters affect the stomatal conductance, and subsequently control Δ in Eq. (1) through changes in the ratios of CO_2 concentration in the ambient atmosphere and intercellular space. The response in discrimination to humidity is further explored in Sect. 3.3.2.

The global average C_3 discrimination varies for the period 1997–2008 with 19 ± 0.15 ‰ year to year (Fig. 2b). Most of this interannual variability (IAV) originates from the mid- and higher latitudes and can be attributed to variations in precipitation and relative humidity as identified by Suits et al. (2005). Over the tropical latitudes the IAV is generally very low. Larger excursions are seen in mixed C_3 and C_4 grid cells in the South American and African subtropics. Shifts in the magnitude of GPP in C_3- and C_4-dominated cells will affect the annual mean discrimination values.

The global annual total discrimination and IAV (assimilation-weighted) is 15.2 ± 0.04 ‰ (linear detrended and averaged for the period 1997–2008), and is, as shown in Table 2, comparable to similar studies (Lloyd and Farquhar, 1994: 14.8‰; Fung et al., 1997: 15.7 ‰; Suits et al., 2005: 15.9 ‰). We see larger differences with the studies of Kaplan et al. (2002) and Scholze et al. (2003). They reported values of 18.1 and 17.7 ‰, respectively, because they assigned 15 and 10 % of the GPP to the less discriminating C_4 plants. In

Table 2. Comparison of isotopic parameters between different modeling studies. The heterotrophic-weighted mean isodisequilibrium coefficient was estimated for the period 1987/88.

	Fraction C_4 GPP (%)	C_3 Δ (‰)	C_4 Δ (‰)	Net Δ (‰)	Isodis. coeff. (1987/1988) (‰)	D_{bio} (1987/1988) (Pg C ‰ yr^{-1})
Lloyd and Farquhar (1994)	21	17.8	3.6	14.8	n/a	n/a
Francey et al. (1995)	n/a	n/a	n/a	18.0	0.43	25.8
Fung et al. (1997)	27	20.0	4.4	15.7	0.33	n/a
Joos and Bruno (1998)	n/a	n/a	n/a	18.7	0.43	26.4
Kaplan et al. (2002)	15	20.0	3 to 4	18.1	n/a	n/a
Scholze et al. (2003 & 2008)	less than 10	10 to 23	3 to 4	17.7	0.42–0.59	23.8–41.8
Suits et al. (2005)	24	19.2	4.4	15.9	n/a	n/a
SiBCASA (this study)	30	19–20	4.4	15.2	0.42	21.2

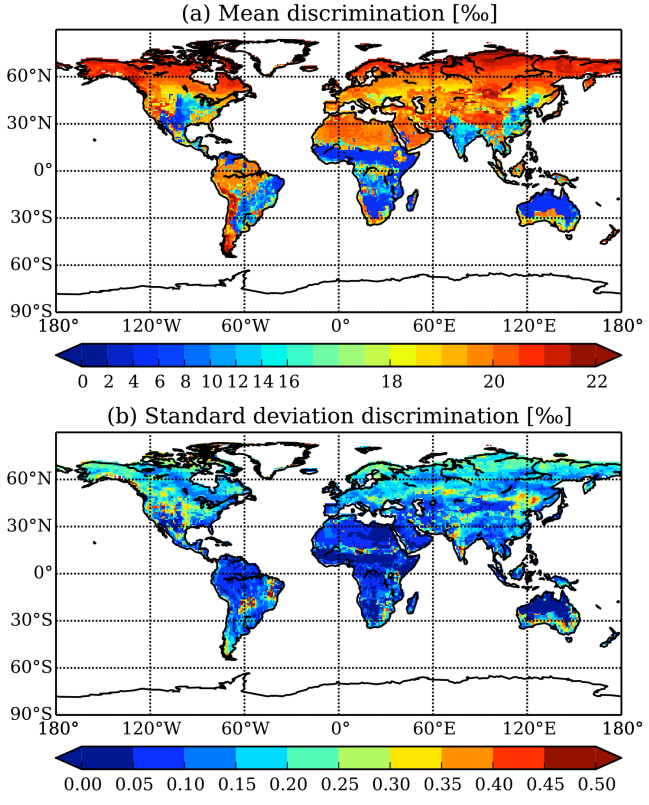

Figure 2. SiBCASA-ISOVAR assimilation-weighted annual plant discrimination **(a)**, from a 13 yr period (1997–2009), and the year-to-year variability (1σ) of the annual discrimination values determined from the same 13 yr period **(b)**. Differences in C_3 and C_4 metabolic pathways give the clear spatial contrast in the annual mean discrimination. Variations in grid-cell-average discrimination are largely driven by RH, precipitation, and soil moisture conditions. The largest standard deviations are found in parts of South America and Africa in mixed C_3/C_4 grid cells, where independent changes in C_3 or C_4 GPP can change grid cell mean discrimination value significantly. Note that the color scale in **(a)** is nonlinear.

contrast, our model assigns around 30 % of the GPP to C_4 plants. These differences mainly depend on the vegetation database used. For instance, our C_3/C_4 distribution database (Still et al., 2003) includes additional C_4 coverage from crop fraction maps (Ramankutty and Foley, 1998), and data on crops from the Food and Agriculture Organization. A large part of the year-to-year changes in global discrimination are driven by shifts in C_3 and C_4 productivity (van der Velde et al., 2013).

3.2 ^{13}C signatures in biosphere–atmosphere exchange

3.2.1 Biomass burning

Because our fire emissions estimates are based on burned-area maps, their spatial patterns are similar but emissions vary widely per unit area burned (van der Werf et al., 2006). As displayed in Fig. 3a, most of the burned area covers Africa and northern Australia, especially in regions dominated by savanna grasses. However, because of their relatively low fuel loads, the actual carbon emissions (Fig. 3b) from these regions are low per unit area burned. Over the period 1997–2009, Australia accounts for 14 % of the total burned area, but it only contributes 4 % of the total fire emissions. Tropical Asia (defined as TransCom region as in Gurney et al., 2002) accounts for just 2 % of the total burned area but emits 13 % of the total global fire emissions. This is mainly due to the high fuel loads in the form of aboveground wood biomass. Africa is by far the largest contributor, both in terms of emissions (53 %) and burned area (70 %). The total is equivalent to 2.55 million $km^2\ yr^{-1}$ of area burned averaged over the period 1997 through 2009.

The annual mean and IAV of the global fire flux for the period 1997–2009 is 1.93 ± 0.40 Pg C yr^{-1}, which is only 0.07 Pg C yr^{-1} lower than reported by CASA-GFED3 (van der Werf et al., 2010). As displayed in Fig. 4, the global trend and the significant IAV in fire emissions are consistent with CASA-GFED3. The SiBCASA model captures the timing of years of strong and weak fire emissions. For instance,

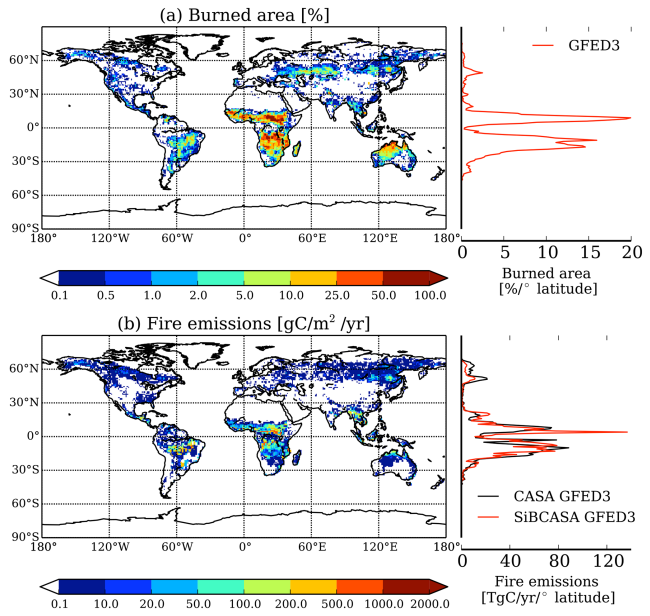

Figure 3. The **(a)** annual burned area (% per $1° \times 1°$) from CASA-GFED3 and **(b)** SiBCASA's fire emissions ($g\,C\,m^{-2}\,yr^{-1}$) averaged over 1997–2009. The color scales in both panels are nonlinear. The panels on the right-hand side display the zonal averages of burned area and fire emissions per degree latitude, respectively. The fire emissions are the product of burned area and the amount of standing biomass (fuel consumption). Neglecting emissions from organic soils explains the underestimation in the Northern Hemisphere compared to CASA-GFED3 (black line).

greater emissions occurred in 1997 and 1998, followed by lower emissions after 1998. We also see the same general regional characteristics, and seasonal and interannual variability as in CASA-GFED3. For instance, Eurasian boreal fluxes are more than twice as large as the North American boreal fluxes because its area is much larger. Globally, 2001 and 2009 are consistently the years with the lowest emissions ($1.5\,Pg\,C\,yr^{-1}$). Some of the year-to-year differences in the annual fire emissions stem from the lack of specific combustion processes in SiBCASA mentioned in the Methodology section, primarily peat and organic soil combustion. Specifically, we underestimate (relative to CASA) the global emissions in 1997, 2002, and 2006 by 0.1–0.3 $Pg\,C\,yr^{-1}$. An example is the fire emissions in tropical Asia, where we miss the peak burning events in 1997, 2002, and 2006 due to the lack of peat burning in our framework. For the other years the emissions between CASA and SiBCASA are very consistent. In the North American boreal, Eurasian boreal and Eurasian temperate regions the emissions are about 50 % lower than estimated by CASA due to lack of organic soil combustion. This is also visible in the zonal mean profile in Fig. 3b. Because these regions contribute only little to the total emissions, it does not affect the global flux much. In tropical and temperate South America the fire emissions are higher throughout the simulation relative to CASA-GFED3. This is a consequence of larger fuel loads in SiBCASA in comparison to CASA, and differences between the coarse biome map and the remotely sensed burned area. These burned-area fields are aggregated from $0.5° \times 0.5°$ resolution to a coarser $1° \times 1°$ resolution. Especially at the boundaries between biome types, e.g., tropical forests (high fuel load) and savannas (low fuel loads), this can give skewed emission because part of the burned area is wrongly assigned to another biome with different simulated biomass. This is apparent close to the Equator, where we observe a large spike in emissions in the zonal mean profile in Fig. 3b. Other minor differences between the flux estimates presented here and those reported in van der Werf et al. (2010) stem from SiBCASA's more simplified representation of the fire parameters. For instance, we used a biome-specific fixed combustion completeness factor rather than a variable one (van Leeuwen et al., 2013).

3.2.2 Disequilibrium

The isodisequilibrium coefficient I_{bio} (combined weighted mean of I_{ba} and I_{fire}) is highly variable in space. Fig. 5a displays the map of the global annual ISOVAR disequilibrium, averaged for the period 1997–2008. Generally, the values of I_{bio} are high in regions where the carbon turnover times are long, such as forests and tundra. The highest values (0.5 ‰) correspond to regions such as boreal forests in North America and Eurasia. The lowest values of I_{bio} can be found in regions covered with herbaceous vegetation such as in the African savanna. Differences in residence times are the result of variations in plant types, respiration, and fire disturbances. Large disequilibria are mostly found in wood, which has the longest aboveground turnover time (30–50 yr). There are no trees in tundra, but the soil carbon is frozen most of the year, which results in effective turnover rates as high as 1500 yr. In our study the total respiration carries the mean signature of old and new carbon. If we were to base I_{bio} solely on heterotrophic respiration, as done in other studies listed in Table 2, its value would become roughly 2 times greater. This is because the δ signature of heterotrophic respiration (2 times lower in magnitude than total respiration) represents an older biomass and is thus heavier in ^{13}C than total respiration, which also includes autotrophic respiration with a δ signature that is much closer to the current assimilation signature.

In 1988 (to compare with other studies), the global heterotrophic-weighted mean I_{bio} was estimated to be 0.42 ‰. This value lies close to the ones found elsewhere for the same year and is summarized in Table 2. For example, Joos and Bruno (1998) and Francey et al. (1995) reported 0.43 ‰, and Scholze et al. (2008) reported a range between 0.42 and 0.59 ‰.

Next we analyze the simulated disequilibrium flux D_{bio}, which in contrast to I_{bio} directly influences the atmospheric

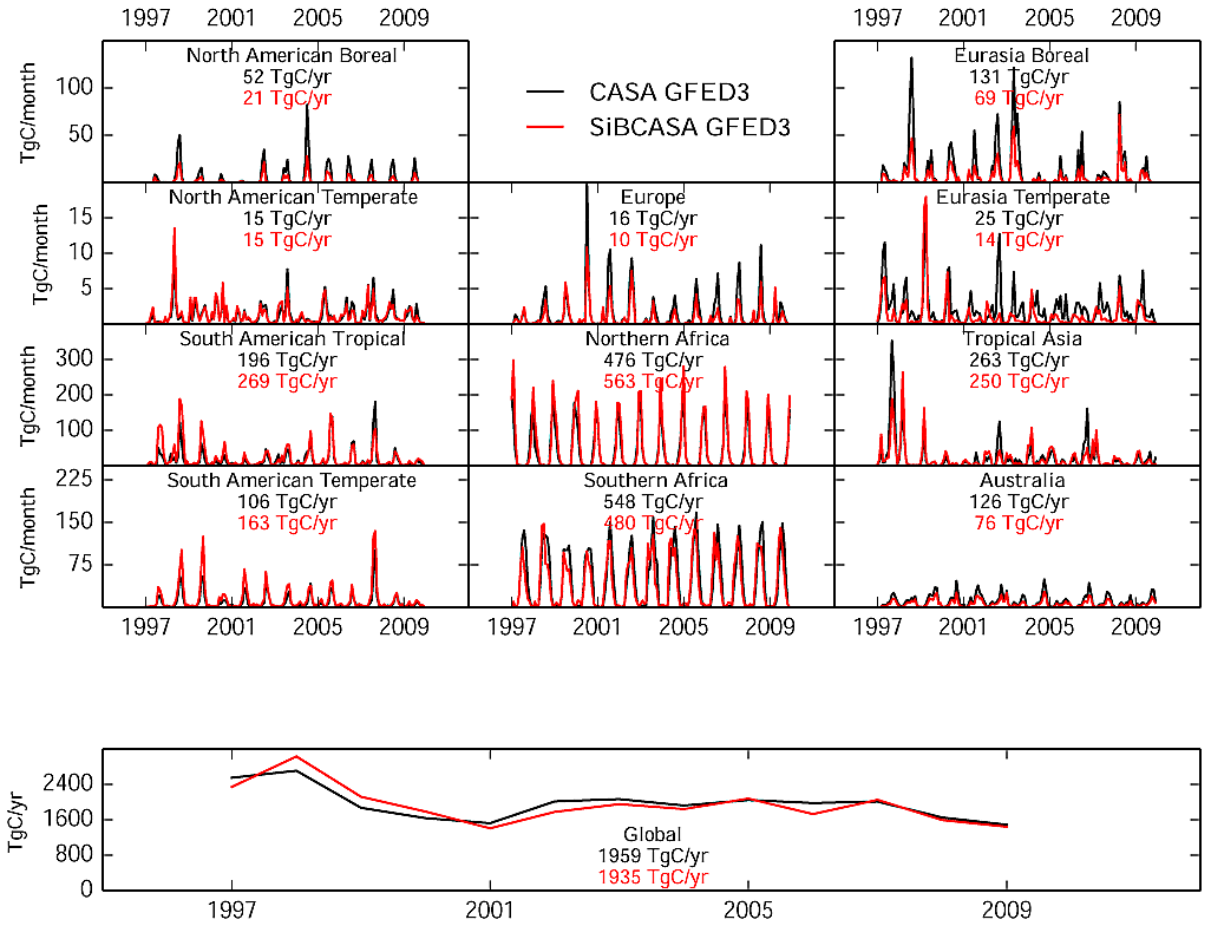

Figure 4. Monthly fire emissions (Tg C month^{-1}) over 1997–2009 for 11 different TransCom regions. CASA-GFED3 (black) is compared to SiBCASA-GFED3 (red) estimates. The multi-year averages for each region are given as values in Tg C yr^{-1}. The regions are geographically ordered, with North American boreal in the top-left panel and Australia in the lower-right panel. Horizontally, the panels share the same y axis. The global annual fire emissions (Tg C yr^{-1}) for both simulations are displayed in the separate panel below.

^{13}C budget. D_{bio} is controlled by both the respiration flux and I_{bio}, which is an integrated parameter of carbon residence time of the different carbon stocks (see Eq. 8). The spatial magnitude of D_{bio} (Fig. 5b) is also clearly different from that of I_{bio} (Fig. 5a). Tropical forests are responsible for 40 % of the total disequilibrium flux. This flux is a combined effect of a large respiration flux (32 % of global respiration) and a relatively long pool turnover ($D_{\mathrm{tropics}} = 10.4$ Pg C ‰ yr^{-1} and $I_{\mathrm{tropics}} = 0.27$ ‰). Around 95 % of this disequilibrium flux originates from heterotrophic respiration, with the remainder from biomass burning. Boreal forest soils are generally older, and thus heavier in ^{13}C, but they account only for 11 % of the total disequilibrium flux ($D_{\mathrm{boreal}} = 2.8$ Pg C ‰ yr^{-1} and $I_{\mathrm{boreal}} = 0.38$ ‰) because productivity and thus respiration are much lower. Therefore, we estimate that the isotopic impact of the boreal regions on the atmosphere is roughly 4 times lower than the impact imposed by the tropical regions. Dry areas with a small amount of biomass such as the American grasslands, African savannas, parts of India, and Australia contribute little to the total disequilibrium flux.

As shown in Fig. 6, from 1950 onward, the atmospheric isotopic composition depleted rapidly in ^{13}C due to intensified emissions of isotopically light CO_2 from fossil fuel combustion. As a response to this depletion, the disequilibrium increased rapidly from 0 Pg C ‰ yr^{-1} in 1950 to 30 Pg C ‰ yr^{-1} at the end of the simulation. The extra variability in δ_{a} after 1989 is from the increase in available flask measurements. Between 1997 and 2008, the two simulations had the following mean values and interannual variability (from the linear trend): ISOVAR, 25.8 ± 1.5 Pg C ‰ yr^{-1}, and ISOVAR-NF, 27.4 ± 1.4 Pg C ‰ yr^{-1}. The ISOVAR-NF experiment, without fire disturbances, resolves generally greater values for D_{bio} than in the other experiment. It confirms that biomass burning shortens the turnover times of the biogeochemical pools, which results in a lower disequilibrium flux than if the turnover is determined only by natural processes, like decay of biomass.

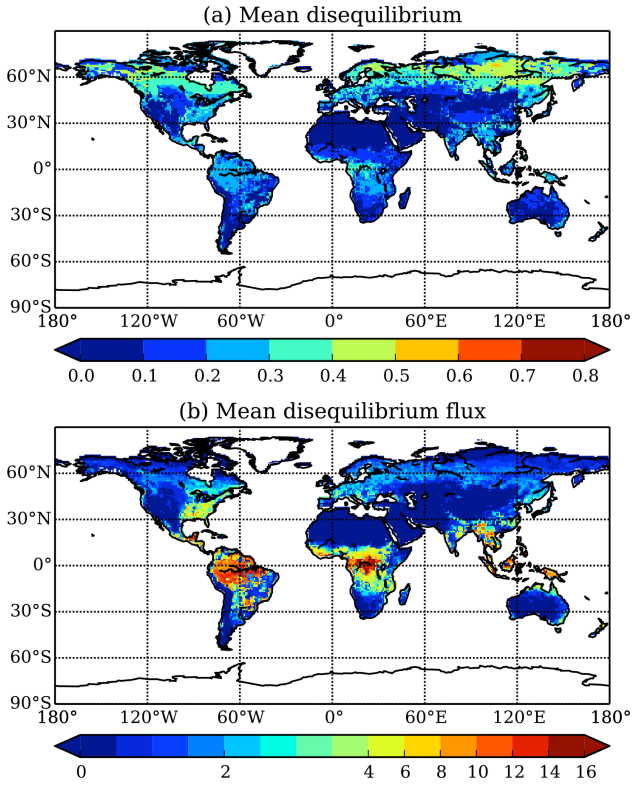

Figure 5. The **(a)** SiBCASA-ISOVAR disequilibrium coefficient (‰) and **(b)** disequilibrium flux (Tg C ‰ cell^{-1} yr^{-1}), averaged for a 12 yr period (1997–2008). Note that the color scale in panel **(b)** is nonlinear.

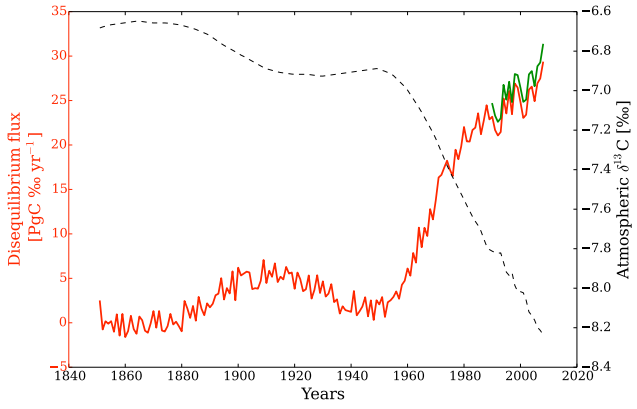

Figure 6. Time series (1851–2008) of the global annual disequilibrium flux for two different experiments: ISOVAR (red) and ISOVAR-NF (green). The ISOVAR-NF simulation is only shown for the period 1990–2008. Since disequilibrium is strongly linked with atmospheric isotopic composition, δ_a (dashed) is added on the secondary y axis.

3.3 Model evaluation with observations

3.3.1 ^{13}C respiration signature

To evaluate our model we use the Biosphere-Atmosphere Stable Isotope Network (BASIN; Pataki et al., 2003). BASIN serves as an archive that uses a common framework for the collection and interpretation of isotopic signatures in CO_2 respiration (δ_r) from Keeling plot intercept data across sites in North and South America.

In general, our simulated δ_r values compare well with the mean observed δ_r values as shown in Fig. 7 for a selection of sites. The vegetation of most of the sites presented here is C_3, which results in a cluster of values with a respiration signature between −23 and −28 ‰. The vegetation at the site in Kansas is predominately C_4 tallgrass prairie, which explains the low value of around −20 ‰. We capture similar signatures in our model, which confirms that there is agreement between actual plant use and the C_4 distribution map from Still et al. (2003). There are also differences between the model and measurements. For example, the simulated respiration signature in the tropical forest site is less negative than observed; for Sisters, Oregon, we see the opposite. The simulated respiration signature is far more negative there than observed. A possible reason is that we misrepresent the carbon age in our model or the fraction of soil respiration. It could be that carbon respired from the soils in SiBCASA is older or younger than measured, and thus substantially more enriched or depleted in ^{13}C as a consequence of the Suess effect. However, it is also possible that we miss external variability in our model, specifically in monthly precipitation, relative humidity, and soil moisture stress. Such environmental conditions can cause more abrupt changes in the respiration signature than currently modeled in SiBCASA. In the next section we investigate this response in more detail for two different locations with measured humidity–^{13}C relationships.

3.3.2 Turnover and humidity response

Several measurement experiments in the past show that C_3 plant discrimination depends strongly on short-term changes in environmental conditions (e.g., Ehleringer and Cook, 1998; Ekblad and Hogberg, 2001; Bowling et al., 2002; Ometto et al., 2002). Atmospheric humidity and soil water stress are considered important factors that, when combined, determine the stomatally induced variations in isotopic discrimination. More importantly, the measurements suggest that it takes only a few days for carbon that is assimilated through photosynthesis to become available again for respiration.

We compare the modeled assimilation-weighted discrimination and the isotopic composition in respiration (δ_r) with the correlation fits determined in measurement experiments by Ekblad and Hogberg (2001) and Bowling et al. (2002). Ekblad and Hogberg measured soil respiration in a boreal forest in northern Sweden and found a strong linear correlation between sampled humidity and the isotopic composition in CO_2 respiration 1–4 days later. This study suggests that

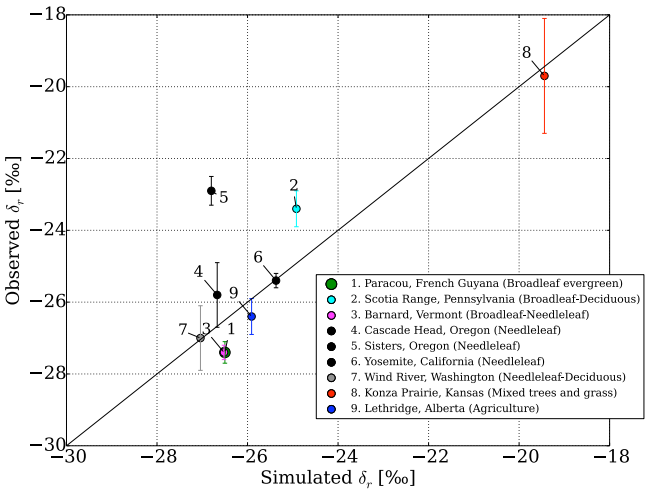

Figure 7. Measured and modeled signature of respiration at nine different sites in North and South America. The measurements are from the BASIN network (Pataki et al., 2003) and were taken in the 1980s and 1990s in the spring and summer months. Each reported value in the figure represents the mean and 1σ standard error over a number of separate measurements which were performed at each particular site, and each simulated value was averaged over the same measurement period. The colors indicate the type of biome each site is part of. Overall, our mean simulated respiration signatures compare well with the observations. Outliers seen in this figure might indicate differences between the prescribed carbon turnover and the actual carbon turnover. It could also indicate SiBCASA's inability to capture drought events that could cause a larger seasonal change in the respiration signature.

a large part of variations in δ_r was caused by respiration of new photosynthate transferred from the foliar by roots, mycorrhizal fungi, and rhizosphere heterotrophs. Bowling et al. (2002) calculated Keeling plot intercepts at four different locations in Oregon. They also found a strong relationship between the 5–10-day lagged δ_r in ecosystem respiration and vapor pressure deficit (VPD). They also suggest that variations in discrimination based on water availability are an important source for this behavior. Henceforth, when we refer to these observations we refer to them by their geographical location: Sweden and Oregon.

Suits et al. (2005) compared SiB's assimilated isotopic signatures with these correlation fits and evaluated the relationship between humidity and discrimination. Because our framework includes the complete exchange of ^{13}C we can expand this analysis with the actual modeled δ_r We use four model simulations to investigate the isotopic signal in respiration: (1) SiBCASA with the single storage pool, (2) SiBCASA with the separate sugar and starch storage pool, (3) SiBCASA with a modified soil moisture stress function, and (4) SiBCASA with a modified humidity stress function. For our simulations we have chosen grid boxes in Oregon and Sweden, which are similar to the locations of the two measurement experiments.

Figure 8a and b show the time series of VPD and discrimination for the single storage pool simulation for a site in Oregon. Day-to-day changes in VPD (Fig. 8a) affects the discrimination almost immediately (Fig. 8b). Discrimination is strongly coupled to CO_2 and water diffusion gradients, which gives higher discrimination for lower VPD values, whereas higher VPD values result in lower discrimination. This relationship between VPD and discrimination is further illustrated in Fig. 9a for simulations at Oregon (blue dots) and Sweden (red dots) in comparison to the approximate curve fits based on measurements (dashed lines). We must stress that these observed relationships in Fig. 9a are an approximation for discrimination because discrimination was not actually measured. Instead, these fits were derived from the respiration signature fit functions shown in Fig. 9b given the current atmospheric isotopic composition δ_a. The modeled discrimination values are in between the two observed relationships, but the general pattern for both locations is more or less the same: a small VPD (high RH) gives greater stomatal conductance, and thus greater discrimination. Strong curvature when the VPD is small, as observed at the Oregon site, is only slightly captured in our model. For the larger VPD regimes, the modeled discrimination reaches a minimum where the slope becomes almost flat, in contrast to the observations.

If we look at the autotrophic respiration the fast changes in VPD are reflected in the observed δ_r but are hardly visible in SiBCASA with the single storage pool (Fig. 8c, green line). The inability to capture the fast-respiring signatures is due to the design of the single storage pool in SiBCASA. Because only 10 % of the storage is readily available for growth, the effective turnover rate of the storage pool is not 7 days but actually 10 times greater, $\sim$ 70 days. This dampens any high frequency changes in the isotope ratio of respiration in contrast to observations. The observed δ_r is derived from the VPD–respiration relationship determined from observations in Oregon (Bowling et al., 2002) and predicts much stronger variations (Fig. 8c, blue dashed line). Note that the strong negative anomaly to -4 ‰ in δ_r when VPD was lower than 0.2 kPa was not actually measured in Oregon.

An improvement is realized when we go to a double storage pool modification (see Sect. 2). It has a substantial effect on δ_r compared to the single storage pool. By allowing carbon extraction from the fast sugar pool, we mimic the transfer of new photosynthates to leaves, wood, and root pools and thus obtain more variations in δ_r to better match with observations in Oregon (Fig. 8c, red line). The standard deviation (1σ) increases almost 4 times in comparison to the single storage pool simulation. Even so, the magnitude of the variations is still 3.5 times lower compared to variations (1σ) that are predicted by the observed VPD–respiration relationship for Oregon. This is not set in stone: if we use a different fit function based on measurements in Sweden (Ekblad and Hogberg, 2001), there is a better match with

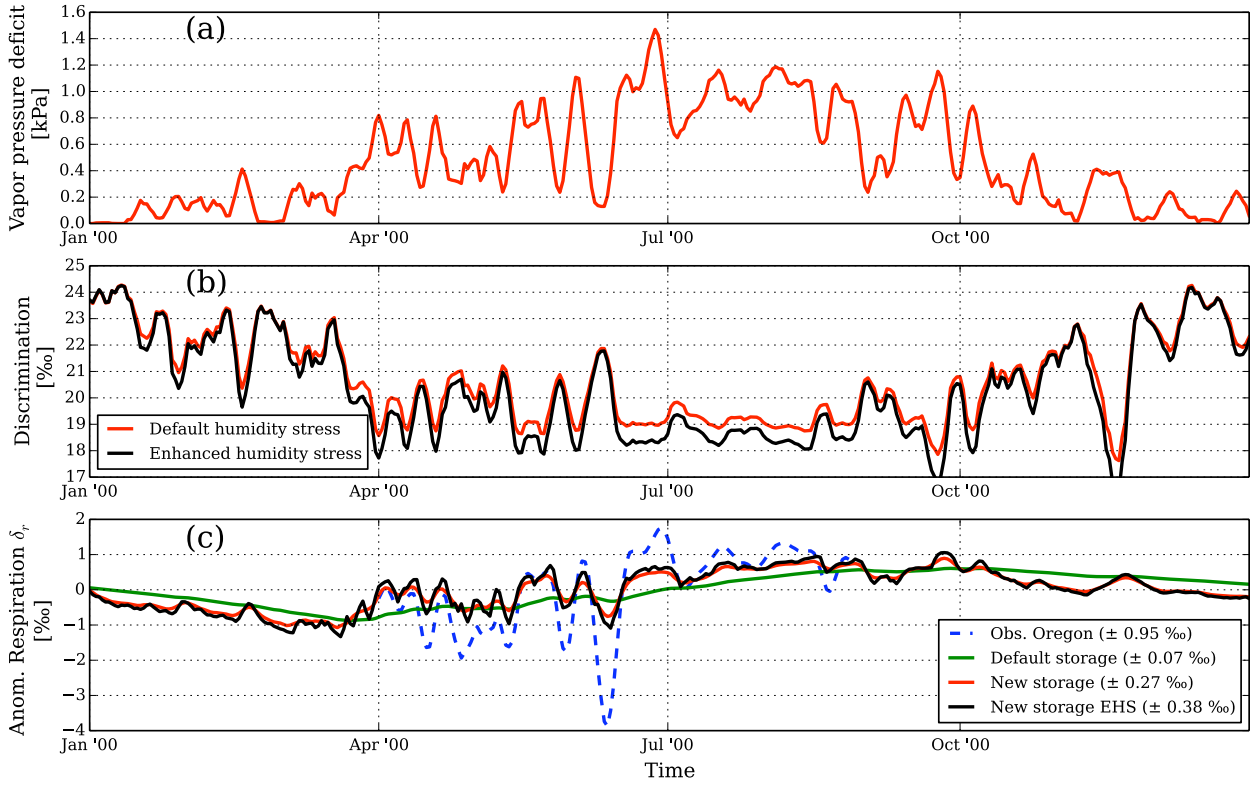

Figure 8. Daily vapor pressure deficit **(a)**, isotopic discrimination **(b)**, and anomalies relative to the mean in the isotopic signature in autotrophic respiration **(c)** for the year 2000 simulated in Oregon. Panel **(c)** depicts the δ_r in respiration from the single storage pool (green line) and the new storage pool structure (red line), and in addition, δ_r predicted with the curve fits determined in Oregon (Bowling et al., 2002, blue dashed line). The 1σ (detrended) variability between April and August is shown in the legend. The estimates due to enhanced humidity stress (EHS) are shown in **(b)** and **(c)** as a black line.

simulated δ_r (simulated variations (1σ) would be twice as low, not shown).

The difference between these two measurement-based VPD–respiration relationships is further illustrated in Fig. 9b. If we look at Oregon and Sweden, we find that the fast sugar pool improves the δ_r relationship for both sites (7-fold slope increase in Sweden and 3-fold slope increase in Oregon). Despite the improvements, variations in δ_r are still limited over the whole VPD range. The new storage pool framework certainly helps to improve the response of δ_r to VPD; however, the amplitude of these variations is underestimated.

An increase of variability in discrimination by changing the soil moisture response curve only has a minor effect on the respiration signal. Soil water stress is one of the different components (alongside irradiation, salinity, and temperature) that affects mesophyll conductance and the CO_2 diffusion inside the plant. In SiBCASA the soil water stress follows a parabolic function of plant available water. There is no stress near field capacity but near wilting point there is a steep drop-off. To change the curve to a linear relationship where stress occurs close to field capacity only has a negligible effect on the discrimination at the sites investigated (not shown).

In a final experiment, we enhanced the stomatal resistance of molecular diffusion from the leaf surface towards the stomatal cavity as a function of humidity. This to mimic a stronger response under drier conditions in discrimination to changes in C_i / C_a, the ratio of CO_2 concentrations in the leaf intercellular spaces to that in the atmosphere. This C_i / C_a ratio is determined by the balance between photosynthetic demand and the stomatal conductance to limit water loss, i.e., a trade-off quantified as the intrinsic water use efficiency (iWUE). In SiBCASA these mechanisms are strongly constrained by the stomatal conductance model and the generalized coefficients for C_3 and C_4 photosynthetic pathways determined in leaf gas-exchange experiments. In reality C_i / C_a differs more strongly among different plant species rather than uniformly in a biome as simulated in SiBCASA. Also the responses in C_i / C_a will differ among different stomatal conductance formulations. Additional responses in C_i / C_a translate onto enhanced changes in discrimination and δ_r. Especially for drier regimes, the outcome of this modification is threefold: extra reduction in C_i / C_a ratio, extra reduction in discrimination, and heavier signatures in δ_r as function of VPD (see Figs. 8b and c, black lines). Moreover, due to these modifications, the

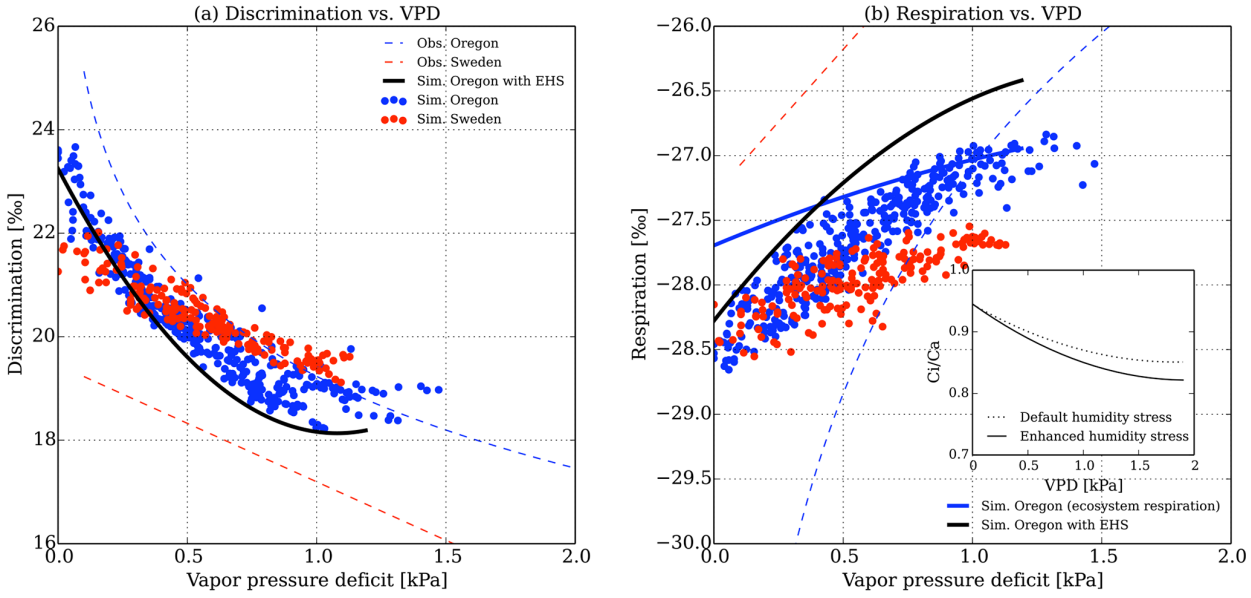

Figure 9. Modeled plant discrimination (‰) and isotopic signature in respiration (‰) as a function of the vapor pressure deficit (VPD, kPa) for two locations: Oregon (blue) and Sweden (red). **(a)** shows discrimination versus VPD. **(b)** shows the isotopic signatures in autotrophic respiration (δ_r) versus VPD. The daily mean values are from the SiBCASA-ISOVAR simulation performed for the months in 2000, 2001, and 2002 when carbon uptake peaked. The daily mean VPD is derived from daylight hours. In **(b)** the blue dashed line represents a logarithmic fit to measured δ_r taken from sites in Oregon (Bowling et al., 2002). The red dashed line represents a linear fit to measured δ_r in a mixed coniferous boreal forest in northern Sweden (Ekblad and Hogberg, 2001). In **(a)** both lines are approximated as plant discrimination using the relationship $\Delta = \frac{\delta_a - \delta_r}{\delta_r/1000+1}$. The solid lines represent curve fits through simulated values at Oregon for ecosystem respiration (blue) and for enhanced humidity stress (black). The inserted panel in **(b)** shows the change in C_i/C_a ratio as a function of VPD due to this additional stress.

VPD–discrimination and respiration relationships, as shown in Figs. 9a and b as black lines, have a 20 % greater slope, which lies much closer to observations in Oregon.

4 Discussion and conclusions

In this study we introduce a modified version of SiBCASA to simulate ^{12}C and ^{13}C exchange. The modifications include realistic fire emissions based on remotely sensed burned area, and the exchange of ^{13}C isotopes between atmosphere and plants. A comprehensive set of observations and other model studies was used to assess the model performance. We present here our main results that emerged from this study.

When we first look at global isotope discrimination we see it is generally consistent with observations and comparable with similar studies. SiBCASA calculates a global annual discrimination of 15.2 ‰ between 1997 and 2008. We do find that the global value depends strongly on the amount of C_4 photosynthesis prescribed in the model.

The global fire emissions compare well with estimates from the CASA-GFED3 study described in van der Werf et al. (2010). Between 1997 and 2009 we simulate an average flux of 1.93 Pg C yr^{-1}, which is 3.5 % less than reported in the CASA-GFED3 study. On both global and regional scales, the trend, the seasonal, and the interannual variability in the fire emissions are consistent. The underestimation of fire emissions in tropical Asia and Boreal regions is expected since our simplified approach does not include specific processes like peat combustion and organic soil combustion. Other smaller discrepancies between SiBCASA and CASA are the result of differences in the amount of biomass and mismatches between the biome type map and the remotely sensed burned area. For future improvements, we will implement processes like peat and organic soil combustion, as well as more specific combustion parameters, which can vary in time and location.

The global disequilibrium signal is consistent with similar studies. There are some notable differences between our disequilibrium flux and the LPJ simulations presented by Scholze et al. (2008). First of all, their disequilibrium flux in the ISOVAR-NF simulation was much larger compared to their ISOVAR simulation ($\sim$ 25 %). This is because their estimates of biomass burning are 4 times higher than ours, which explains the large impact on the disequilibrium flux in their study. They do, however, acknowledge that their global mean value of biomass burning (8 Pg C yr^{-1}) is much higher compared to many other studies (e.g., van der Werf et al., 2003). The differences in the mean ISOVAR disequilibrium isofluxes between Scholze et al. (34.8 Pg C ‰ yr^{-1}) and this

study (25.8 Pg C ‰ yr^{-1}) at the end of the simulation period is a consequence of differences in the amount of C_4 plant growth and differences in the resolved heterotrophic respiration fluxes between the two studies: 69.4 Pg C yr^{-1} compared to 52.3 Pg C yr^{-1} in our study. We note that our disequilibrium flux magnitude, together with a reasonable estimate of ocean disequilibrium, remains nearly 30 % too low to close the atmospheric δ_a budget (also see Langenfels et al., 1999), and thus remains an outstanding issue in the global carbon balance. To increase the estimates of the global disequilibrium flux we would simultaneously need a decrease in turnover rates and an increase in carbon pool sizes to enhance respiration, but this needs to be investigated more thoroughly in the future. This is a good example of how ^{13}C in atmospheric CO_2 can eventually help us to constrain multiple processes within a biogeochemical model like SiBCASA.

Another source of uncertainty, which is not included in the model, is land use change. As presented by Scholze et al. (2008), land use change can have a large impact on the disequilibrium flux. Especially the gradual increase of low-discriminating C_4 plant activity (pastures and crops) caused a reduction of 40 % in the disequilibrium flux compared their ISOVAR simulation (without cultivation). Our simulations assumed a static C_4 fraction map from Still et al. (2003), which is representative of the situation in the 1980s and 1990s. Because of its gradual nature, land use change is likely not a large source of variability in disequilibrium. Instead, most of the variability comes from year-to-year changes in discrimination and changes in C_3 and C_4 productivity (van der Velde et al., 2013). We also did not include the mobilization and decay of harvested wood biomass (for instance furniture). Nevertheless, such influences certainly deserve more attention in SiBCASA and will be a subject for future improvements.

Atmospheric humidity appears as an important contributor to the stomatally induced variations in isotopic discrimination, and these findings are in agreement with various measurements published in the literature. The humidity in the atmosphere affects stomatal conductance, which is reflected in discrimination, and ultimately alters the isotopic content of CO_2 respired back to the atmosphere. In the model we observe (1) a generally weak response in discrimination to changes in VPD, (2) latency in recently assimilated carbon to become available for respiration, (3) possibly the absence of additional processes that contribute to additional stomatal stress, and (4) the absence of additional isotope effects that contribute to variability in respired CO_2 isotopic composition. We made an important advancement by separating sugars and starch in the SiBCASA pool configuration. The gradient between the isotopic signature in respiration and humidity as shown in the observations increased 3- to 7-fold. Nevertheless, the variations in respiration are dampened compared the variations in discrimination as a function of humidity. This dampening effect in isotopic response is a consequence of the carbon in the storage pools being transferred back and forth between usable sugars ($\sim$ 7-day turnover) and starch ($\sim$ 60-day turnover) in order to keep the ratio between both pools close to 1 : 9. This transfer dilutes the isotopic signal from photosynthetic discrimination and this process may in reality be less dominant than currently modeled in SiBCASA. The 1 : 9 constraint is likely too extreme for the growing season as the ratio of sugar to starch varies more strongly over the season. The ratio will be higher at the start of the growing season, when plants convert a lot of starch to sugar to grow the new leaves. The observed ^{13}C relationships therefore suggest the need for a bigger pool of fast-respiring carbon.

Exchanging the simulated autotrophic respiration for ecosystem respiration (autotrophic + heterotrophic) in Fig. 9b gives slightly less negative isotope ratios (solid blue slope) because CO_2 of decomposing soil organic matter (SOM) is generally more enriched due to the Suess effect. In addition, we see additional dampening in the variability because of the decomposing SOM in SiBCASA exhibits very little variability compared to recently fixed photosynthates. This is interesting because the measured relationships in Oregon, which show a very strong response to humidity, were determined with Keeling plot intercepts that reflect the ecosystem respiration (thus including SOM decomposition). It is possible that we miss important dynamic changes in heterotrophic substrates that can influence the isotopic composition of soil respiration. But it also possible that the contribution from SOM decomposition (heterotrophic respiration) was larger in the model than the contribution from SOM respiration during the measurements presented in the literature. Also, the chosen sampling strategies for the Keeling plot method can influence the footprint. Sampling δ_a at different heights can reflect different mixtures of atmospheric CO_2 dominated by either plant respiration or soil respiration (Pataki et al., 2003).

Other discrimination effects after photosynthesis are not implemented in SiBCASA when carbon is allocated to the different carbon pools or when carbon is respired back to the atmosphere. However, in reality, there are numerous additional isotope effects after photosynthetic uptake that affect the isotopic composition of different carbon compounds inside the plant, but they are often very complex to model and their responses to changes in environmental conditions are not fully understood (Brüggemann et al., 2011). In addition, no significant discrimination effects were found in respiratory processes (Lin and Ehleringer, 1997). Any other isotope effects will cause variations in the isotopic composition of carbon that is converted into different compounds. These discrimination effects are likely an additional source of variations in the isotope ratios of respiration but are currently not accounted for in the model.

A stronger gradient (20 %) in the isotopic composition of respiration towards humidity can be achieved with a slightly modified C_i / C_a ratio and iWUE to acquire more variability in discrimination. This modification is not to invalidate the

stomatal conductance formulation using isotope measurements. Instead, it investigates what δ_r in respiration would look like if the model responds more strongly to changes in VPD, and explores the possibilities that the response to humidity in stomatal conductance and discrimination might not be strong enough, especially when VPD may become large. We want to stress that these changes were only tested for two specific locations. To scale these changes in stomatal conductance and iWUE to a global domain is probably not justified as it is likely that they are only applicable for certain biomes under certain conditions.

This study shows that the isotopic composition of plants can change under influence of environmental conditions and discrimination processes. To simulate ^{13}C exchange more accurately, a double storage pool with a fast turnover component is an important addition to a biogeochemical model. The study also highlights the importance of ^{13}C to help assess and improve the simulation of biogeochemical processes such as the allocation and turnover of carbon and the responses to drought. Measurements suggest that responses to climate anomalies will likely invoke more variability in the assimilation and respiration signatures than what we currently model, but it can also indirectly invoke more variability in the isotopic disequilibrium. This is important because the discrimination and disequilibrium flux play a critical role in the total atmospheric ^{13}C budget and its variability. Our next step focusses on the implementation of the SiBCASA framework (with biomass burning and ^{13}C exchange) with a data-assimilation system to interpret observed signals in atmospheric CO_2 and δ_a with regard to changes in terrestrial exchange and drought response.

Appendix A: Isotopic notation

Isotopes in a given sample are usually expressed as ratio R: a rare compound to an abundant compound. In the case of ^{13}C,

$$R = \frac{\text{rare}}{\text{abundant}} = \frac{^{13}C}{^{12}C}. \quad \text{(A1)}$$

In nature, differences in ratios between samples are often very small. Therefore, sampled isotopic ratios are compared to a common standard ratio, which is measured in carbonate rock Pee Dee belemnite (PDB). Deviations from the standard are expressed in per mill (‰), and are defined as

$$\delta^{13}C_{\text{sample}} = \left(\frac{\left[^{13}C/^{12}C\right]}{\left[^{13}C/^{12}C\right]_{\text{std}}} - 1 \right) \times 1000 \quad \text{(A2)}$$
$$= \left(\frac{R_{\text{sample}}}{R_{\text{std}}} - 1 \right) \times 1000,$$

where $R_{\text{std}} = 0.0112372$ (PDB standard; Craig, 1957). That means that roughly 1.1 % of the carbon exists in the form of ^{13}C. Negative values of $\delta^{13}C$ indicate that the isotopic ratio R_{sample} is smaller than the PDB standard, i.e., the sample is more depleted in ^{13}C. If $\delta^{13}C$ is positive the sample is more enriched in ^{13}C.

During certain processes (e.g., photosynthesis), isotopic ratios can change due to influence of molecular diffusion or chemical reactions. For instance, the isotopic ratio in recent assimilated carbon in a plant is smaller than the isotopic ratio of carbon in atmospheric CO_2 ($R_{\text{ab}} < R_{\text{atm}}$). This effect is also called isotopic discrimination and it can be expressed as the ratio of $R_{\text{atm}}/R_{\text{ab}}$. Discrimination is often expressed in per mill, just like for the isotopic signatures in samples, i.e.,

$$\Delta = \left(\frac{R_{\text{atm}}}{R_{\text{ab}}} - 1 \right) \times 1000 \approx \delta^{13}C_{\text{atm}} - \delta^{13}C_{\text{ab}}, \quad \text{(A3)}$$

and is often a desirable notation because strength of discrimination between samples can be approximated by the difference in isotopic signatures. If $R_{\text{atm}}/R_{\text{ab}} = 1$, which means that the isotopic signatures in both samples are the same, this would give $\Delta = 0$ ‰ (no discrimination). On the other hand, if $R_{\text{atm}}/R_{\text{ab}} > 1$, we would compute $\Delta > 0$ ‰.

Acknowledgements. We thank all the people involved in the BASIN measurement campaigns as well as Louis Giglio for sharing the GFED version 3 burned-area data. This project was funded and supported by a VIDI grant (864.08.012) and a grant for computing time (SH-060-13) from the Netherlands Organisation for Scientific Research (NWO).

Edited by: R. Keeling

References

Alden, C. B., Miller, J. B., and White, J. W. C.: Can bottom-up ocean CO_2 fluxes be reconciled with atmospheric ^{13}C observations?, Tellus B, 62, 369–388, doi:10.1111/j.1600-0889.2010.00481.x, 2010.

Ballantyne, A. P., Miller, J. B., and Tans, P. P.: Apparent seasonal cycle in isotopic discrimination of carbon in the atmosphere and biosphere due to vapor pressure deficit, Global Biogeochem. Cy., 24, GB3018, doi:10.1029/2009GB003623, 2010.

Barbaroux, C. and Breda, N.: Contrasting distribution and seasonal dynamics of carbohydrate reserves in stem wood of adult ring-porous sessile oak and diffuse-porous beech trees, Tree Physiol., 22, 1201–1210, 2002.

Bowling, D. R., McDowell, N. G., Bond, B. J., Law, B. E., and Ehleringer, J. R.: ^{13}C content of ecosystem respiration is linked to precipitation and vapor pressure deficit, Oecologia, 131, 113–124, 2002.

Bowling, D. R., Pataki, D. E., and Randerson, J. T.: Carbon isotopes in terrestrial ecosystem pools and CO_2 fluxes, New Phytol., 148, 24–40, 2008.

Brugnoli, E. and Farquhar, G. D.: Photosynthetic fractionation of carbon isotopes, in: Photosynthesis: Physiology and Metabolism, edited by: Leegood, R. C., Sharkey, T. D., and von Caemmerer, S., Kluwer Acad., Norwell, Mass., 399–434, 2000.

Brüggemann, N., Gessler, A., Kayler, Z., Keel, S. G., Badeck, F., Barthel, M., Boeckx, P., Buchmann, N., Brugnoli, E., Esperschütz, J., Gavrichkova, O., Ghashghaie, J., Gomez-Casanovas, N., Keitel, C., Knohl, A., Kuptz, D., Palacio, S., Salmon, Y., Uchida, Y., and Bahn, M.: Carbon allocation and carbon isotope fluxes in the plant-soil-atmosphere continuum: a review, Biogeosciences, 8, 3457–3489, doi:10.5194/bg-8-3457-2011, 2011.

Ciais, P., Tans, P. P., White, J., and Trolier, M.: Partitioning of ocean and land uptake of CO_2 as inferred by $\delta^{13}C$ measurements from the NOAA climate monitoring and diagnostics laboratory global air sampling network, J. Geophys. Res., 100, 5051–5070, 1995.

Collatz, G. J., Ball, J., Grivet, C., and Berry, J. A.: Physiological and environmental regulation of stomatal conductance, photosynthesis and transpiration: a model that includes a laminar boundary layer, Agr. Forest Meteorol., 54, 107–136, 1991.

Collatz, G. J., Ribas-Carbo, M., and Berry, J. A.: Coupled photosynthesis-stomatal conductance model for leaves of C4 plants, Aust. J. Plant Physiol., 19, 519–538, 1992.

Craig, H.: The geochemistry of stable carbon isotopes, Geochim. Cosmochim. Ac., 3, 53–92, 1953.

Craig, H.: Isotopic standards for carbon and oxygen and correction factors for mass-spectrometric analysis of carbon dioxide, Geochim. Cosmochim. Ac., 12, 133–149, 1957.

Ehleringer, J. R. and Cook, C. S.: Carbon and oxygen isotope ratios of ecosystem respiration along an Oregon conifer transect: preliminary observations based upon small-flask sampling, Tree Physiol., 18, 513–519, 1998.

Ekblad, A. and Hogberg, P.: Natural abundance of ^{13}C in CO_2 respired from forest soils reveals speed of link between tree photosynthesis and root respiration, Oecologia, 127, 305–308, 2001.

Farquhar, G. D.: On the nature of carbon isotope discrimination in C_4 species, Aust. J. Plant Physiol., 10, 205–226, 1983.

Farquhar, G. D., Caemmerer, S. V., and Berry, J. A.: A biochemical-model of photosynthetic CO_2 assimilation in leaves of C_3 species, Planta, 149, 78–90, 1980.

Farquhar, G. D., Ehleringer, J. R., and Hubrick, K. T.: Carbon isotope discrimination and photosynthesis, Annu. Rev. Plant Phys., 40, 503–537, 1989.

Francey, R. J., Tans, P. P., Allison, C. E., Enting, I. G., White, J. W. C., and Trolier, M.: Changes in oceanic and terrestrial carbon uptake since 1982, Nature, 373, 326–330, 1995.

Francey, R. J., Allison, C. E., Etheridge, D. M., Trudinger, C. M., Enting, I. G., Leuenberger, M., Langenfelds, R. L., Michel, E., and Steele, L. P.: A 1000-year high precision record of delta C-13 in atmospheric CO_2, Tellus B, 51, 170–193, 1999.

Fung, I., Field, C. B., Berry, J. A., Thompson, M. V., Randerson, J. T., Malmström, C. M., Vitousek, P. M., James Collatz, G., Sellers, P. J., Randall, D. A., Denning, A. S., Badeck, F., and John, J.: Carbon 13 exchanges between the atmosphere and biosphere, Global Biogeochem. Cy., 11, 507–533, 1997.

Gaucher, C., Gougeon, S., Mauffette, Y., and Messier, C.: Seasonal variation in biomass and carbohydrate partitioning of understory sugar maple (Acer saccharum) and yellow birch (Betula alleghanienis) seedlings, Tree Physiol., 25, 93–100, 2005.

Giglio, L., Randerson, J. T., van der Werf, G. R., Kasibhatla, P. S., Collatz, G. J., Morton, D. C., and DeFries, R. S.: Assessing variability and long-term trends in burned area by merging multiple satellite fire products, Biogeosciences, 7, 1171–1186, doi:10.5194/bg-7-1171-2010, 2010.

Gurney, K. R., Law, R. M., Denning, A. S., Rayner, P. J., Baker, D., Bousquet, P., Bruhwiler, L., Chen, Y. H., Ciais, P., Fan, S., Fung, I. Y., Gloor, M., Heimann, M., Higuchi, K., John, J., Maki, T., Maksyutov, S., Masarie, K., Peylin, P., Prather, M., Pak, B. C., Randerson, J., Sarmiento, J., Taguchi, S., Takahashi, T., and Yuen, C. W.: Towards robust regional estimates of CO_2 sources and sinks using atmospheric transport models, Nature, 415, 626–630, 2002.

Indermuhle, A., Stocker, T. F., Joos, F., Fischer, H., Smith, H. J., Wahlen, M., Deck, B., Mastroianni, D., Tschumi, J., Blunier T., Meyer, R., and Stauffer, B. : Holocene carbon-cycle dynamics based on CO_2 trapped in ice at Taylor Dome, Antarctica, Nature, 398, 121–126, 1999.

Joos, F. and Bruno, M.: Long-term variability of the terrestrial and oceanic carbon sinks and the budgets of the carbon isotopes C-13 and C-14, Global Biogeochem. Cy., 12, 277–295, 1998.

Kaplan, J. O., Prentice, I. C., and Buchmann, N.: The stable carbon isotope composition of the terrestrial biosphere: modeling at scales from the leaf to the globe, Global Biogeochem. Cy., 16, 1060, doi:10.1029/2001GB001403, 2002.

Keeling, C. D.: The Suess effect: 13Carbon–14Carbon interrelations, Environ. Int., 2, 229–300, 1979.

Keeling, C. D. and Revelle, R.: Effects of El Nino/Southern Oscillation on the atmospheric content of carbon dioxide, Meteoritics, 20, 437–450, 1985.

Keeling, C. D., Bacastow, R. B., Carter, A. F., Piper, S. C., Whorf, T. P., Heimann, M., Mook, W. G., and Roeloffzen, H.: A three-dimensional model of atmospheric CO_2 transport based on observed winds: 1. Analysis of observational data, in: Aspects of Climate Variability in the Pacific and the Western Americas, edited by: Peterson, D. H., American Geophysical Union, Washington DC, USA, 165–236, 1989.

Langenfels, R. L., Michel, E., Steele, L. P.: A 1000-year high precision record of $\delta^{13}C$ in atmospheric CO_2, Tellus B, 51, 170–193, 1999.

Lin, G. and Ehleringer, J. R.: Carbon isotopic fractionation does not occur during dark respiration in C_3 and C_4 plants, Plant Physiol., 114, 391–394, 1997.

Lloyd, J. and Farquhar, G. D.: ^{13}C discrimination during CO_2 assimilation by the terrestrial biosphere, Oecolgia, 99, 201–215, 1994.

Masarie, K. A. and Tans, P. P.: Extension and integration of atmospheric carbon-dioxide data into a globally consistent measurement record, J. Geophys. Res.-Atmos., 100, 11593–11610, 1995.

Mook, W. G., Bommerson, J. G., and Staverman, W. H.: Carbon isotope fractionation between dissolved bicarbonate and gaseous carbon dioxide, Earth Planet. Sc. Lett., 22, 169–176, 1974.

Nakazawa, T., Morimoto, S., Aoki, S., and Tanaka, M.: Time and space variations of the carbon isotopic ratio of tropospheric carbon dioxide over Japan, Tellus B, 45, 258–274, 1993.

O'Leary, M. H.: Carbon isotope fractionation in plants, Phytochemistry, 20, 553–567, 1981.

O'Leary, M. H.: Measurement of the isotopic fractionation associated with diffusion of carbon dioxide in aqueous solution, J. Phys. Chem., 88, 823–825, 1984.

Ometto, J. P. H. B., Flanagan, L. B., Martinelli, L. A., Moreira, M. Z., Higuchi, N., and Ehleringer, J. R.: Carbon isotope discrimination in forest and pasture ecosystems of the Amazon Basin, Brazil, Global Biogeochem. Cy., 16, 1109, doi:10.1029/2001GB001462, 2002.

Page, S. E., Siegert, F., Rieley, J. O., Boehm, H. D. V., Jaya, A., and Limin, S.: The amount of carbon released from peat and forest fires in Indonesia during 1997, Nature, 420, 61–65, doi:10.1038/nature01131, 2002.

Pataki, D. E., Ehleringer, J. R., Flanagan, L. B., Yakir, D., Bowling, D. R., Still, C. J., Buchmann, N., Kaplan, J. O., and Berry, J. A.: The application and interpretation of Keeling plots in terrestrial carbon-cycle research, Global Biogeochem. Cy., 17, 1022, doi:10.1029/2001GB001850, 2003.

Peters, G. P., Marland, G., Quere, C. L., Boden, T., Canadell, J. G., and Raupach, M. R.: Rapid growth in CO_2 emissions after the 2008–2009 global financial crisis, Nat. Clim. Change, 2, 2–4, 2012.

Piispanen, R., and Saranpaa, P.: Variation of non-structural carbohydrates in silver birch (Betula pendula Roth) wood, Trees, 15, 444–451, doi:10.1007/s004680100125, 2001.

Potter, C. S., Randerson, J. T., Field, C. B., Matson, P. A., Vitousek, P. M., Mooney, H. A., and Klooster, S. A.: A process-oriented model based on global satellite and surface data, Global Biogeochem. Cy., 7, 811–842, 1995.

Ramankutty, N. and Foley, J. A.: Characterizing patterns of global land use: an analysis of global croplands data, Global Biogeochem. Cy., 12, 667–686, 1998.

Randerson, J. T., Thompson, M. V., Malmstrom, C. M., Field, C. B., and Fung, I. Y.: Substrate limitations for heterotrophs: implications for models that estimate the seasonal cycle of atmospheric CO_2, Global Biogeochem. Cy., 10, 585–602, 1996.

Rayner, P. J., Law, R. M., Allison, C. E., Francey, R. J., Trudinger, C. M., and Pickett-Heaps, C.: Interannual variability of the global carbon cycle (1992–2005) inferred by inversion of atmospheric CO_2 and $\delta^{13}CO_2$ measurements, Global Biogeochem. Cy., 22, GB3008, doi:10.1029/2007GB003068, 2008.

Schaefer, K., Collatz, G. J., Tans, P. P., Denning, A. S., Baker, I., Berry, J. A., Prihodko, L., Suits, N., and Philpott, A.: Combined Simple Biosphere/Carnegie-Ames-Stanford Approach terrestrial carbon cycle model, J. Geophys. Res., 113, G03034, doi:10.1029/2007JG000603, 2008.

Scholze, M., Kaplan, J. O., Knorr, W., and Heimann, M.: Climate and interannual variability of the atmosphere-biosphere $^{13}CO_2$ flux, Geophys. Res. Lett., 30, 1097, doi:10.1029/2002GL015631, 2003.

Scholze, M., Ciais, P., and Heimann, M.: Modeling terrestrial ^{13}C cycling: climate, land use and fire, Global Biogeochem. Cy., 22, GB1009, doi:10.1029/2006GB002899, 2008.

Sellers, P. J., Tucker, C. J., Collatz, G. J., Los, S. O., Justice, C. O., Dazlich, D. A., and Randall, D. A.: A global 1 by 1 NDVI data set for climate studies – Part 2: The generation of global fields of terrestrial biosphysical parameters from NDVI, Int. J. Remote. Sens., 15, 3519–3545, 1994.

Sellers, P. J., Randall, D. A., Collatz, G. J., Berry, J. A., Field, C. B., Dazlich, D. A., Zhang, C., Collelo, G. D., and Bounoua, L.: A revised land surface parameterization (SiB2) for atmospheric GCMs – Part 1: Model formulation, J. Climate, 9, 676–705, 1996a.

Sellers, P. J., Los, S. O., Tucker, C. J., Justice, C. O., Dazlich, D. A., Collatz, G. J. and Randall, D. A.: A revised land surface parameterization (SiB2) for atmospheric GCMs – Part 2: The generation of global fields of terrestrial biophysical parameters from satellite data, J. Climate, 9, 706–737, 1996b.

Siegenthaler, U. and Oeschger, H.: Biospheric CO_2 emissions during the past 200 years reconstructed by deconvolution of ice core data, Tellus B, 39, 140–154, 1987.

Still, C. J., Berry, J. A., Collatz, G. J., and DeFries, R. S.: Global distribution of C-3 and C-4 vegetation: carbon cycle implications, Nature Climate Change, 17, 1006–1019, 2003.

Suess, H. E.: Radiocarbon concentration in modern wood, Science, 122, 415–417, 1955.

Suits, N., Denning, A., Berry, J., and Still, C.: Simulation of carbon isotope discrimination of the terrestrial biosphere, Global Biogeochem. Cy., 19, GB1017, doi:10.1029/2003GB002141, 2005.

Tans, P. P.: On calculating the transfer of C-13 in reservoir models of the carbon-cycle, Tellus, 32, 464–469, 1980.

Tans, P. P., Berry, J. A., and Keeling, R. F.: Oceanic $^{13}C/^{13}C$ observations – a new window on ocean CO_2 uptake, Global Biogeochem. Cy., 7, 353–368, 1993.

van der Velde, I. R., Miller, J. B., Schaefer, K., Masarie, K. A., Denning, S., White, J. W. C., Tans, P. P., Krol, M. C., and Peters, W.: Biosphere model simulations of interannual variability in terres-

trial 13C/12C exchange, Global Biogeochem. Cy., 27, 637–649, 2013.

van der Werf, G. R., Randerson, J. T., Collatz, G. J., and Giglio, L.: Carbon emissions from fires in tropical and subtropical ecosystems, Glob. Change Biol., 9, 547–562, 2003.

van der Werf, G. R., Randerson, J. T., Giglio, L., Collatz, G. J., Kasibhatla, P. S., and Arellano Jr., A. F.: Interannual variability in global biomass burning emissions from 1997 to 2004, Atmos. Chem. Phys., 6, 3423–3441, doi:10.5194/acp-6-3423-2006, 2006.

van der Werf, G. R., Randerson, J. T., Giglio, L., Collatz, G. J., Mu, M., Kasibhatla, P. S., Morton, D. C., DeFries, R. S., Jin, Y., and van Leeuwen, T. T.: Global fire emissions and the contribution of deforestation, savanna, forest, agricultural, and peat fires (1997–2009), Atmos. Chem. Phys., 10, 11707–11735, doi:10.5194/acp-10-11707-2010, 2010.

van Leeuwen, T. T., Peters, W., Krol, M. C., van der Werf, G. R.: Dynamic biomass burning emission factors and their impact on atmospheric CO mixing ratios, J. Geophys. Res.-Atmos., 118, 6797–6815, 2013.

Vidale, P. L. and Stockli, R.: Prognostic canopy air space solutions for land surface exchanges, Theor. Appl. Climatol., 80, 245–257, 2005.

Wingate, L., Ogee, J., Burlett, R., Bosc, A., Devaux, M., Grace, J., Loustau, D., and Gessler, A.: Photosynthetic carbon isotope discrimination and its relationship to the carbon isotope signals of stem, soil and ecosystem respiration, New Phytol., 188, 576–589, 2010.